# Structural ( n , m ) Determination of Isolated Single-Wall Carbon Nanotubes by Resonant Raman Scattering

# Structural $(n, m)$ Determination of Isolated Single-Wall Carbon Nanotubes by Resonant Raman Scattering

A. Jorio,[1] R. Saito,[5] J. H. Hafner,[6] C. M. Lieber,[6] M. Hunter,[2] T. McClure,[3] G. Dresselhaus,[4] and M. S. Dresselhaus[1,*]

[1]*Department of Physics, Massachusetts Institute of Technology, Cambridge, Massachusetts 02139*
[2]*Department of Earth, Atmospheric and Planetary Sciences, Massachusetts Institute of Technology, Cambridge, Massachusetts 02139*
[3]*Center for Materials Science, Massachusetts Institute of Technology, Cambridge, Massachusetts 02139*
[4]*Francis Bitter Magnet Laboratory, Massachusetts Institute of Technology, Cambridge, Massachusetts 02139*
[5]*Department of Electronic-Engineering, University of Electro-Communications, Tokyo, 182-8585 Japan*
[6]*Department of Chemistry, Harvard University, Cambridge, Massachusetts 02138*

(Received 14 August 2000)

We show that the Raman scattering technique can give complete structural information for one-dimensional systems, such as carbon nanotubes. Resonant confocal micro-Raman spectroscopy of an $(n, m)$ individual single-wall nanotube makes it possible to assign its chirality uniquely by measuring one radial breathing mode frequency $\omega_{\mathrm{RBM}}$ and using the theory of resonant transitions. A unique chirality assignment can be made for both metallic and semiconducting nanotubes of diameter $d_t$, using the parameters $\gamma_0 = 2.9$ eV and $\omega_{\mathrm{RBM}} = 248/d_t$. For example, the strong RBM intensity observed at 156 $\mathrm{cm}^{-1}$ for 785 nm laser excitation is assigned to the $(13, 10)$ metallic chiral nanotube on a $Si/SiO_2$ surface.

DOI: 10.1103/PhysRevLett.86.1118 PACS numbers: 78.30.Na, 63.22.+m, 78.66.Tr

Much effort has been devoted to improving the methods of nanotube production, and significant progress has been made to narrow the diameter distribution of nanotubes produced by different catalysts and growth processes [1]. However, there is as yet no method for selecting a specific chirality in the nanotube production process, since the nanotube structural energy is only weakly dependent on chirality [2]. Consequently, actual nanotube samples appear to exhibit a homogeneous chirality distribution. Thus the development of techniques to assign a chirality $(n, m)$ to a given single-wall carbon nanotube (SWNT) is very important for the development of both future technological applications and scientific studies. Resonant confocal micro Raman spectroscopy (RCMRS) provides a powerful technique to study the quantum properties of electrons and phonons in carbon nanotubes [3], and to identify the nanotube diameters $(d_t)$ in a sample containing a mixture of chiralities. We show here how RCMRS can give the complete $(n, m)$ atomic structural assignment for an isolated SWNT.

Isolated SWNTs were prepared by a chemical vapor deposition method on a Si substrate containing nanometer size iron catalyst particles. The Si substrate was oxidized to have a thin $SiO_2$ surface coating and, in this case, we do not expect significant charge transfer between the SWNTs and the substrate. Since the nanotubes nucleate and grow from well isolated catalyst particles, nanotube bundles are not formed. We have transferred these nanotubes from the surface to AFM probe tips and have confirmed that they are individual single-walled tubes by transmission electron microscopy [4]. Figure 1 shows an atomic force microscopy (AFM) image of one of our samples exhibiting a concentration of $6 \pm 3$ SWNTs per $\mu\mathrm{m}^2$. Most nanotubes are individual SWNTs, but a few of them are entangled with each other, showing a "Y" shape in some AFM images. The inset to Fig. 1 shows the wide diameter distribution of the sample ($\sim 1 < d_t < \sim 3$ nm). The accuracy of the AFM diameter measurement is $\pm 0.2$ nm at most. Resonant Raman spectra from 100 to 1900 $\mathrm{cm}^{-1}$ were obtained from single isolated SWNTs on this substrate, using a Kaiser Optical Systems, Hololab 5000R: Modular Research Micro-Raman Spectrograph (1 $\mu$m laser spot) with 25 mW power, and $E_\ell = 785$ nm $= 1.58$ eV laser line excitation.

Figure 2 shows several typical Raman spectra, each taken from one resonant nanotube on the Si substrate. Inset (a) shows the spectrum obtained from one spot on the sample (Fig. 1), with Raman signals from the Si substrate at 303, 521, and 963 $\mathrm{cm}^{-1}$ [5], used for the intensity calibration. Inset (b) shows a zoom for the 1200–1800 $\mathrm{cm}^{-1}$

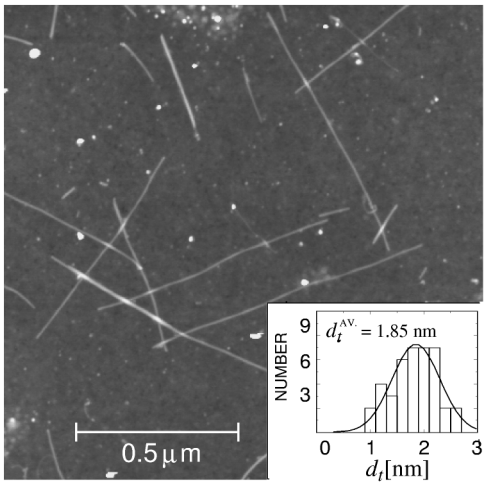


FIG. 1. AFM images of the sample. The small particles are iron catalysts. The inset shows the diameter distribution of the sample taken from 40 observed SWNTs.

 0031-9007/01/86(6)/1118(4)$15.00 

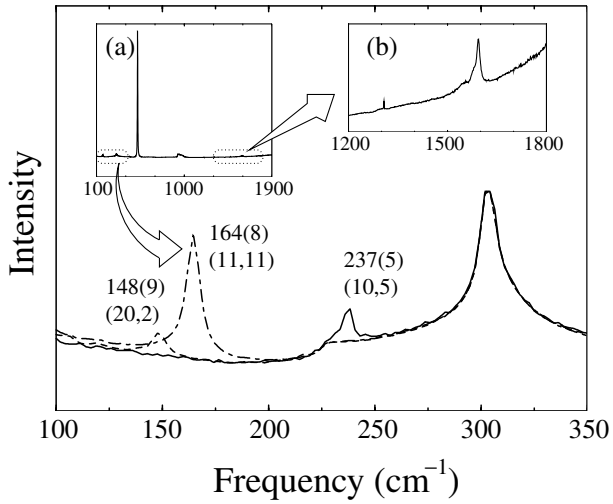


FIG. 2. Raman spectra from three different spots on the Si substrate, showing only one resonant nanotube and one RBM frequency for each of 3 spots. The RBM frequencies (widths) and $(n, m)$ assignment for each resonant SWNT are displayed. The 303 cm$^{-1}$ feature comes from the Si substrate. Inset (a) shows Raman spectra from one spot on the sample, including 303, 521, and 963 cm$^{-1}$ Raman features from the Si substrate. Inset (b) shows a zoom of the corresponding $G$-band region.

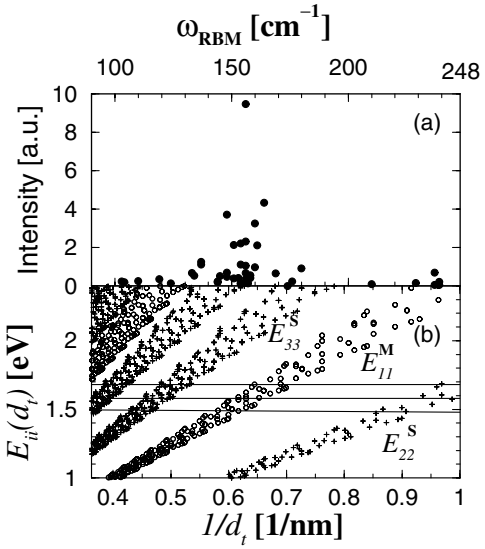


FIG. 3. (a) Measured frequency vs intensity for the RBM peaks observed at 42 different spots on the sample (Fig. 1). (b) Calculated energy separation $E_{ii}$ as a function of $1/d_t$, $\gamma_0 = 2.9$ eV, and $\omega_{\mathrm{RBM}} = 248/d_t$. Circles are for metallic SWNTs ($E_{ii}^{\mathrm{M}}$), and crosses for semiconducting SWNTs ($E_{ii}^{\mathrm{S}}$).

frequency region, where we observe the nanotube tangential $G$-band modes. The main part of Fig. 2 shows a zoom for the low frequency region (100–350 cm$^{-1}$), where we observe the 303 cm$^{-1}$ peak from the Si substrate and the nanotube radial breathing modes (RBM). The RBM intensity is comparable to that of the quasi-3D Si film because of the large 1D resonant Raman enhancement effect in the nanotubes. The three spectra come from three different spots on the substrate, showing the presence of only one resonant nanotube and one RBM frequency for each spot, with $\omega_{\mathrm{RBM}} = 148$, 164, and 237 cm$^{-1}$ for the three spots, each exhibiting natural line widths of 5–10 cm$^{-1}$ [6,7]. As discussed below, looking at the frequency and intensity of the RBM features in the RCMRS spectra, it is possible to uniquely assign $(n, m)$ values to the observed resonant SWNTs [see $(n, m)$ assignment on Fig. 2] based on theory.

Figure 3(a) shows a plot of the measured frequency vs intensity for the RBM peak observed at 42 different spots where we found resonant SWNTs. Figure 3(a) has 47 points, since we occasionally observe the appearance of 2 or even 3 RBMs at a single light spot. The surprising appearance of sufficient Raman intensity for a Raman signal from an isolated SWNT is due to the resonance condition for Raman spectroscopy that is obtained when an energy separation $E_{ii}$ between van Hove singularities (vHs) [8,9] is close to the laser excitation energy $E_\ell = 1.58$ eV. Therefore, although the sample has a relatively large density of isolated SWNTs ($6 \pm 3$ SWNTs per laser spot), the probability of finding a SWNT in resonance with the $E_\ell = 1.58$ eV laser line is only about $1/10$. Many spots on the sample must be measured before we find a resonant Raman signal from one isolated SWNT.

Figure 3(b) shows a plot of the energy separations $E_{ii}$ between the vHs for a given $(n, m)$ SWNT as a function of $1/d_t$. The vHs in the density of states (DOS) are calculated using the tight binding calculation with the parameters $\gamma_0 = 2.9$ eV and $a_{\mathrm{C-C}} = 0.144$ nm, which reproduces the resonant Raman spectra of SWNTs very well [9,10]. The SWNTs predicted to be resonant must have $E_{ii}$ within a resonant window $E_\ell \pm 0.10$ eV. Figures 3(a) and 3(b) can be correlated since $\omega_{\mathrm{RBM}} = \alpha/d_t$. With the value $\alpha \sim 248$ cm$^{-1}$ nm, we obtain good agreement between the observed resonant RBM frequencies and calculated values for $\omega_{\mathrm{RBM}}$ from the $E_{11}^{\mathrm{M}}$ and $E_{ii}^{\mathrm{S}}$ ($i = 2$, 3, and 4 for semiconducting SWNTs) interband transitions (see Fig. 3). In fact, when we vary $\alpha$ by 5%, we no longer obtain good agreement with our measured $\omega_{\mathrm{RBM}}$ data.

The assignment of only *one* SWNT is needed for a precise determination of $\alpha$. We here show that this is possible by analyzing the observed RBM intensities. In the present single nanotube spectroscopy experiment, the DOS is that of an individual nanotube, and the DOS is highly singular. Because of the trigonal warping effect [9], each interband transition $E_{ii}^{\mathrm{M}}$ for metallic SWNTs is split into two DOS peaks, and there are two resonant conditions for each chiral ($0 < \theta < 30°$) or zigzag ($\theta = 0°$) nanotube. The separation between DOS peaks decreases with increasing $\theta$, and is zero for armchair nanotubes ($\theta = 30°$) [9,11]. Thus an especially large Raman intensity is expected when: (i) an $E_{ii}$ is close to $E_\ell$, *and* when (ii) the DOS splitting is small. Thus, armchair or chiral nanotubes with a large chiral angle ($\theta$ near 30°) have a higher probability for giving the strongest signal in the single nanotube Raman experiment among the different chiralities in the resonant energy window ($E_\ell \pm 0.1$ eV).

Figure 3(a) shows one unusually high intensity RBM peak at $\omega_{\mathrm{RBM}} = 156\ \mathrm{cm}^{-1}$. This peak should obey the two conditions given above for large intensity. Considering theory, the observed highest intensity $\omega_{\mathrm{RBM}} = 156\ \mathrm{cm}^{-1}$ comes from a metallic SWNT. When we select metallic nanotubes [where $n - m$ in $(n, m)$ is a multiple of 3] and the resonant window is $1.48 < E_{11}^{\mathrm{M}} < 1.68$ eV, 17 different chiralities are found theoretically, corresponding to 14 different calculated $\omega_{\mathrm{RBM}}$ frequencies that, for $\alpha = 248\ \mathrm{cm}^{-1}\,\mathrm{nm}$, are in the range $\sim 144 < \omega_{\mathrm{RBM}} < 174\ \mathrm{cm}^{-1}$, as listed in Table I. This is consistent with the experiments where 12 different frequencies in the range $144 < \omega_{\mathrm{RBM}} < 176\ \mathrm{cm}^{-1}$ within $\pm 1\ \mathrm{cm}^{-1}$ experimental accuracy are identified from Raman spectra taken at 42 different light spots. Since it is not always possible in our experiment to find all possible chiralities for a finite number of light spots, the number of experimental modes should always be smaller than the theoretical number. Table I shows that there are two armchair nanotubes, (11, 11) and (12, 12), within this resonant window, with $E_{11}^{\mathrm{M}} = 1.63$ and 1.50 eV, respectively. These values are not very close to $E_\ell$ and the first condition for high intensity is not satisfied. Furthermore, using $\alpha = 248\ \mathrm{cm}^{-1}\,\mathrm{nm}$, their calculated $\omega_{\mathrm{RBM}}$ are 164.0 and 150.3 $\mathrm{cm}^{-1}$, respectively, that are not close to the most intense peak observed at 156 $\mathrm{cm}^{-1}$. Among the 17 different chiralities in Table I, there are only a few nanotubes with large chiral angles $\theta > 20°$. When we use $\gamma_0 = 2.9$ eV, the two $E_{11}^{\mathrm{M}}$ singularities for (13, 10) are 1.58 and 1.55 eV. One of the $E_{11}^{\mathrm{M}}$ values agrees very well with $E_\ell$, and the other is also close. Therefore, it is reasonable to assign the (13, 10) chirality to the strongest observed intensity peak at 156 $\mathrm{cm}^{-1}$. The parameter of 248 $\mathrm{cm}^{-1}\,\mathrm{nm}$ in $\omega_{\mathrm{RBM}} = 248/d_t$ is thus determined, so that the $\omega_{\mathrm{RBM}}$ value for the (13, 10) nanotube becomes 156.3 $\mathrm{cm}^{-1}$. Furthermore, the empirical parameter of 248 $\mathrm{cm}^{-1}\,\mathrm{nm}$ is justified by the other intense $\omega_{\mathrm{RBM}}$ features with $E_{11}^{\mathrm{M}}$ closer to $E_\ell$ as shown in bold face in Table I [see also Fig. 3(a)]. Therefore, the assignment of this *one* SWNT gives us a value for $\alpha$, which is consistent with $(n, m)$ assignments for all the other 37 RBMs that are observed (both in frequency and intensity). This assignment is unique in the sense that there is no alternative choice of $(n, m)$ for explaining the large number of observed Raman frequencies and their relative intensities.

We emphasize here that we do not compare the calculated and experimental intensities quantitatively, since the measured intensity depends on the nanotube length and exact position of the experimental laser spot. In fact, in the experiment, we get 7 different intensities at 156 $\mathrm{cm}^{-1}$ for 7 different spots. A difference in intensity is expected since: (1) the nanotube lengths, at different light spots, are different from one another, and (2) tubes having different chiralities, such as (17, 5) and (13, 10), with different $E_{11}^{\mathrm{M}}$ splittings, still can have the same $\omega_{\mathrm{RBM}}$. When we get very strong experimental peaks, this means that the corresponding nanotube has an $E_{11}^{\mathrm{M}}$ close to $E_\ell$.

For higher $\omega_{\mathrm{RBM}}$ values (>200 $\mathrm{cm}^{-1}$), semiconducting nanotubes are resonant and the number of chiralities is limited because of the small $d_t$ values. When we select semiconducting nanotubes with $1 < d_t < 3$ nm subject to the resonant window condition $1.48 < E_{22}^{\mathrm{S}} < 1.68$ eV, we get 8 possible chiralities. In the experiment we observed

TABLE I. Possible chiralities predicted for metallic nanotubes and their calculated $\omega_{\mathrm{RBM}}$ in the resonant window $1.48 < E_{11}^{\mathrm{M}} < 1.68$ eV. We also display the observed $\omega_{\mathrm{RBM}}$, with the number of times each appears between parentheses.

| $(n, m)$ | $d_t$ [nm] | $\theta$ [deg] | $\omega_{\mathrm{RBM}}$ [$\mathrm{cm}^{-1}$][a] (calc.) | (expt.) | $E_{11}^{\mathrm{M}}$[a,b] [eV] | | |
|---|---|---|---|---|---|---|---|
| (18, 6) | 1.72 | 13.9 | 144.4 | 144(2) | 1.49 | | 1.40 |
| (19, 4) | 1.69 | 9.4 | 146.8 | ⋯ | 1.53 | | 1.42 |
| (20, 2) | 1.67 | 4.7 | 148.3 | ⋯ | **1.55** | | 1.42 |
| (21, 0) | 1.67 | 0.0 | 148.8 | **148**(5)[c] | **1.56** | | 1.43 |
| (15, 9) | 1.67 | 21.8 | 148.8 | ⋯ | 1.51 | | 1.46 |
| (12, 12) | 1.65 | 30.0 | 150.3 | **151**(3) | | 1.50 | |
| (16, 7) | 1.62 | 17.3 | 153.0 | **154**(5) | **1.57** | | 1.49 |
| (17, 5) | 1.59 | 12.5 | 156.4 | **156**(6) | **1.62** | | 1.51 |
| (13, 10) | 1.59 | 25.7 | 156.4 | **156**(1) | **1.58** | | **1.55** |
| (18, 3) | 1.56 | 7.6 | 158.8 | 158(1) | 1.66 | | 1.52 |
| (19, 1) | 1.55 | 2.5 | 160.0 | **160**(3) | 1.68 | | **1.54** |
| (14, 8) | 1.53 | 21.1 | 162.0 | ⋯ | 1.65 | | **1.58** |
| (11, 11) | 1.51 | 30.0 | 164.0 | **164**(1) | | 1.63 | |
| (15, 6) | 1.49 | 16.1 | 166.7 | **165**(1) | 1.72 | | **1.62** |
| (16, 4) | 1.46 | 10.9 | 170.4 | 169(1) | 1.79 | | 1.64 |
| (17, 2) | 1.44 | 5.5 | 172.7 | 174(1) | 1.81 | | 1.65 |
| (18, 0) | 1.43 | 0.0 | 173.5 | 176(1) | 1.83 | | 1.65 |

[a]Bold face indicates a strong intensity [see Fig. 3(a)].
[b]Two $E_{11}^{\mathrm{M}}$ values for each *chiral* $(n, m)$ SWNT are also given.
[c]Ambiguity of the assignment occurs between (20, 2) and (21, 0).

4 different $\omega_{\mathrm{RBM}}$ frequencies. This result is reasonable, first because of the smaller number of possible chiralities, and second because of the fewer small diameter nanotubes in the sample (see inset to Fig. 1). In Table II we list $\omega_{\mathrm{RBM}}$ values for semiconducting nanotubes. The experimental values of 210, 229, 237, and 239 $\mathrm{cm}^{-1}$ for $\omega_{\mathrm{RBM}}$ are assigned with no adjustable parameters to the (14, 1), (11, 4), (10, 5), and (8, 7), respectively. Again the agreement (Table II) is excellent, since five of the six observed SWNTs are expected to be strongly resonant, and are thus easier to find. The value $\alpha = 248\ \mathrm{cm}^{-1}\,\mathrm{nm}$ and a unique $(n, m)$ assignment from $\omega_{\mathrm{RBM}}$ is again confirmed.

Unique $(n, m)$ assignments with Raman spectroscopy could not be made for SWNTs with large $d_t$. By increasing $d_t$ (decreasing $\omega_{\mathrm{RBM}}$), the number of resonant SWNTs within the resonant window increases, making a unique $(n, m)$ assignment difficult. For lower observed $\omega_{\mathrm{RBM}}$ values (below 136 $\mathrm{cm}^{-1}$), we calculate and find 48 semiconducting $(n, m)$ for $\omega_{\mathrm{RBM}} > 100\ \mathrm{cm}^{-1}$ within our resonant window. However, when we select the energy window $1.48 < E_{ii}^{\mathrm{S}} < 1.68$ eV $(i = 3, 4)$, the corresponding $\omega_{\mathrm{RBM}}$ range goes up to 132 $\mathrm{cm}^{-1}$, consistent with experimental observations up to 136 $\mathrm{cm}^{-1}$ [see Fig. 3(a)].

Since the assignments of $\omega_{\mathrm{RBM}}$ for many metallic and semiconducting nanotubes are very good, we conclude that the experimental value $\alpha = 248\ \mathrm{cm}^{-1}\,\mathrm{nm}$, based on the theoretical assignment of $\omega_{\mathrm{RBM}} = 156\ \mathrm{cm}^{-1}$ for the (13, 10) chiral nanotube, is justified. This experimental empirical value is larger than the previously published value ($\alpha = 223.75\ \mathrm{cm}^{-1}\,\mathrm{nm}$ [12]) due to limitations on force constant model calculations, in which the force constants are taken from those of graphite. This 10% difference in $\alpha$ might be due to interlayer interactions, or to interactions between the nanotubes with air or with the substrate. These possible interaction mechanisms require further investigation with regard to their effect on $\alpha$. Though the value of $\alpha = 248\ \mathrm{cm}^{-1}\,\mathrm{nm}$ should be used for samples similarly prepared and on similar substrates, other sample preparation methods and substrates may require a small change in the $\alpha$ value. What is shown in the present work, is a proper evaluation of $\alpha$ leads to a unique determination of $(n, m)$ for a single isolated SWNT by measuring $\omega_{\mathrm{RBM}}$ through the RCMRS technique in conjunction with theory. A method for evaluating the reliability of the determination of $\alpha$ is also presented.

TABLE II. Possible chiralities predicted for semiconducting nanotubes and their $\omega_{\mathrm{RBM}}$ (calculated and observed) in the resonant window $1.48 < E_{22}^{\mathrm{S}} < 1.68$ eV.

| $(n, m)$ | $d_t$ [nm] | $\theta$ [deg] | $\omega_{\mathrm{RBM}}$ [$\mathrm{cm}^{-1}$] (calc.) | (expt.) | $E_{22}^{\mathrm{S}}$[a] [eV] |
|---|---|---|---|---|---|
| (14, 1) | 1.15 | 3.4 | 215.1 | 210(1) | 1.50 |
| (10, 6) | 1.11 | 21.8 | 223.1 | ⋯ | 1.51 |
| (9, 7) | 1.10 | 25.9 | 224.9 | ⋯ | 1.48 |
| (11, 4) | 1.07 | 14.9 | 232.2 | 229(1) | **1.60** |
| (10, 5) | 1.05 | 19.1 | 236.1 | 237(2) | **1.54** |
| (12, 2) | 1.04 | 7.6 | 238.2 | ⋯ | 1.66 |
| (8, 7) | 1.03 | 27.8 | 240.3 | 239(2) | **1.61** |
| (11, 3) | 1.01 | 11.7 | 244.7 | ⋯ | **1.57** |

[a]Bold face indicates a strong resonance.

In future work, use of a marked $Si/SiO_2$ substrate will allow us to mark the position of the light spot, so that the (13, 10) chirality could be observed directly by an STM measurement, thus providing independent confirmation of the theory. We can also check our theoretical prediction by using another laser excitation energy on the same sample. However, it should be mentioned here that a good resonant condition for carbon nanotubes is not always obtained using a given laser energy. The selection of $E_\ell = 1.58$ eV (785 nm) provides a convenient window that is well matched for both semiconducting and metallic nanotubes in a sample containing a large $d_t$ distribution. However, if we had used a sample with a narrow diameter distribution around $1.38 \pm 0.10$ nm, the laser excitation of 1.58 eV would become silent, with no nanotubes predicted to be resonant within the observable window [10].

In conclusion, here we show that in the case of one-dimensional physics, Raman scattering from one carbon nanotube can independently provide its complete $(n, m)$ structural information. Making $(n, m)$ SWNT assignments with the Raman technique can result in a major advance for future SWNTs studies. For example, using this approach, transport measurements could be performed on a number of SWNTs, each of which have been independently characterized for their $(n, m)$ values.

This work utilized MRSEC Shared Facilities supported by the National Science Foundation (No. DMR-9400334) and NSF Laser Facility Grant No. 9708265-CHE. The authors thank Dr. S. D. M. Brown and Mr. S. Cronin for help. In addition, A. J. acknowledges financial support from CNPq–Brazil, and R. S. acknowledges a Grant-in-Aid (No. 11165216) from the Ministry of Education, Japan. MIT authors acknowledge NSF Grants No. DMR 98-04734 and No. INT 98-15744.

*On leave.

[1] R. Saito *et al.,* Appl. Phys. Lett. **60**, 2204 (1992).
[2] J. W. Mintmire and C. T. White, Carbon **33**, 893 (1995).
[3] M. S. Dresselhaus and P. C. Eklund, Adv. Phys. **49**, 705 (2000).
[4] J. H. Hafner, C. L. Cheung, T. H. Oosterkamp, and C. M. Lieber, J. Phys. Chem. B (to be published).
[5] P. A. Temple and C. E. Hathaway, Phys. Rev. B **7**, 3685 (1973).
[6] G. S. Duesberg *et al.,* Chem. Phys. Lett. **310**, 8 (1999).
[7] K. Kneipp *et al.,* Phys. Rev. Lett. **84**, 3470 (2000).
[8] H. Kataura *et al.,* Synth. Met. **103**, 2555 (1999).
[9] R. Saito, G. Dresselhaus, and M. S. Dresselhaus, Phys. Rev. B **61**, 2981 (2000).
[10] M. Milnera *et al.,* Phys. Rev. Lett. **84**, 1324 (2000).
[11] P. Kim *et al.,* Phys. Rev. Lett. **82**, 1225 (1999).
[12] S. Bandow *et al.,* Phys. Rev. Lett. **80**, 3779 (1998).